Microstructural and Tribological Properties of Al_2O_3-13pctTiO$_2$ Thermal Spray Coatings Deposited by Flame Spraying

RASSIM YOUNES, MOHAND AMOKRANE BRADAI, ABDELHAMID SADEDDINE, YOUCEF MOUADJI, ALI BILEK, and ABDERRAHIM BENABBAS

THe present investigation has been conducted to study the tribological properties of Al_2O_3-13pctTiO$_2$ (AT-13) ceramic coatings deposited on a low carbon steel type E335 by using a thermal flame spray technique. The microstructure and phase composition of wire and coatings were analyzed by scanning electron microscope, energy dispersive spectroscopy (EDS), and X-ray diffraction (XRD). Measurements of micro hardness were also performed on the surface of the coatings. The tribological tests were carried out using a pin-on-disk tribometer at different loads. All tests were performed using two disks as counter body, namely Al_2O_3-ZrO$_2$ (AZ-25) and Al_2O_3-TiO$_2$ (AT-3) which formed couple 1 and couple 2, respectively, in order to work out the wear rate and friction coefficient. Roughness profiles were also evaluated before and after each test. The SEM showed that the dense microstructure of Al_2O_3-TiO$_2$ (AT-13) coatings have a homogenous lamellar morphology and complex of several phases with the presence of porosities and unmelted particles. The XRD analysis of the wire before the spray showed a majority phase of α-Al$_2$O$_3$ rhombohedral structure and a secondary phase of Al$_2$TiO$_5$ orthorhombic structure with little traces of TiO$_2$ (rutile) tetragonal structure, whereas the XRD of the coating revealed the disappearance of TiO$_2$ replaced by the formation of a new metastable phase γ-Al$_2$O$_3$ cubic structure. The tribological results showed that the applied contact pressure affects the variation of the friction coefficient with time and that it decreases with the rise of the normal force of contact. It was found also that the couple 2 with nearly chemical compositions of spray-coated (AT-13) and disk (AT-3) exhibited much higher wear resistance than the couple 1 although they have sliding coefficient of friction nearly.

I. INTRODUCTION

THE use of coatings for protection against wear and corrosion has a long history. In this context, thermal spray is a technique that produces a wide range of coatings for diverse applications. It involves introducing solid particles (wire or powder) in a flame or plasma jet to melt and accelerate them before they come crashing on the substrate where they form a multilayer.[1–3] Thermal spraying of ceramic coatings is an important method of protecting various metallic parts, which are exposed to very hard environments. Hard ceramic coatings are very good candidates for anti-wear and anti-corrosion applications.[4–8] Sprayed Alumina (Al_2O_3) or alumina-titania (Al_2O_3-TiO$_2$) coatings have the potential for improvements in the mechanical properties depending on enhancements of physical properties resulting from the microstructure characteristics.[9–11] They are fairly porous, which can be useful under harsh working environments.[12–17] Thermal spray coatings processes, that include plasma, wire-arc, flame and high velocity oxygen fuel, have attracted considerable attention due to their versatile nature and adaptability to spray almost any kind of coating powder (ceramic, metallic, polymeric, or composite) onto almost any substrate material. The use of thermal spray flame wire was initially limited to electric current conductor materials. But, recently new materials have been developed in the form of cored-wires, filled with reinforced alloy powders, ceramic particles is also possible. These cored-wires allow the making of coatings of super alloys and cermets in order to improve the tribological properties.[18] Fervel et al.[19] reported that the coatings wear resistance achieved by plasma deposition from the Al_2O_3-40pctTiO$_2$ powder (AT-40) was higher than that of deposits developed using powders of Al_2O_3-13pctTiO$_2$ (AT-13). In contrary, Habib et al.[20] concluded that the higher hardness of coatings (AT-13) obtained by

RASSIM YOUNES, Research Scholar, and MOHAND AMOKRANE BRADAI and ABDELHAMID SADEDDINE, Assistant Professors, are with the Laboratory of Mechanics, Materials and Energetic, Faculty of Technology, University of Bejaia, 06000 Bejaia, Algeria. Contact e-mail: mokbrad@yahoo.fr YOUCEF MOUADJI, Assistant Professor, is with the Laboratory of Mechanics, Faculty of Engineering Sciences, Campus Chaabet-Ersas, University of Constantine, 25000 Constantine, Algeria. ALI BILEK, Professor, is with the Mechanical Laboratory of Structure and Energetic, Mechanical Engineering Department, University of Tizi-Ouzou, 15000 Tizi-Ouzou, Algeria. ABDERRAHIM BENABBAS, Professor, is with the Laboratory Processes for Materials, Energy, Water and Environment, Faculty of Science and Technology, University of Bouira, 10000 Bouira, Algeria.
Manuscript submitted March 9, 2015.
Article published online July 14, 2015.

oxyacetylene flame was the reason that these coatings were more resistant to abrasive wear by sliding contact such as those developed with powders (AT-40). In another study, Ahn et al.[21] found that low wear resistance of coatings (AT-13) made with conventional micrometric powders is due to the presence of brittle phases from titanium oxide produced between the splats of multilayers.

In this paper, the aim of this investigation has been conducted in order to clear focus on aspects related to the structure, microstructure, and mechanical properties of coatings ceramic Al_2O_3-TiO_2 (AT-13) deposited on a low carbon steel type E335 by thermal flame spray technique. The choice of these ceramics coatings aims to improve the wear resistance of the renovated mechanical parts to give it again a new technical life despite its previous degradation in service. The microstructure, phase structure, elements distribution, and microhardness of the coatings are studied. Roughness profiles were also recorded before and after each test. The influence of the applied load and sliding time on the friction coefficient and wear resistance of the coatings are discussed as two contact couples:

– Couple 1: Pin coated with Al_2O_3-TiO_2 (AT-13)/ ceramic disk Al_2O_3-ZrO_2 (AZ-25).
– Couple 2: Pin coated with Al_2O_3-TiO_2 (AT-13)/ ceramic disk Al_2O_3-TiO_2 (AT-3).

II. EXPERIMENTAL DETAILS

A. Materials Used

The substrate used in the present investigation was an E335 steel with the following nominal chemical composition (wt pct) obtained by using analysis X-rays fluorescence which is represented in Table I.

Before the coating process, the surface of the substrate was grit blasted with corundum particles of 99.50 wt pct purity and 0.5 mm mean particle size, using an air of 0.4 MPa, an incidence angle of 90 deg and a gun-to-substrate distance of 150 mm. The surface was then cleaned and degreased using acetone within an ultrasonic bath. The grit blasted substrates were coated with wire form of 4.75 mm diameter of alumina alloy reinforced with 13 pct titanium oxide (AT-13). This wire was flame sprayed onto grit blasted substrate using an oxygen- acetylene gun. The coatings subsequently deposited had average thickness 0.8 to 1 mm. The chemical composition of coatings and two disks used as counter body in tribological tests are shown in Table II.

B. Process and Spray Conditions

The development of the metal coatings required to use a gun flame-wire type Master-Jet Gun 2 (Figure 1) with low speed electric motors (10 mm/s) for driving the wire.

A gas control system consists on flowmeter for controlling the flow of oxygen and acetylene and manometers regulating the pressure of flame gas, air. During projection, the gun was positioned perpendicular to the surface of the substrates at a controlled distance of about 150 mm. A compressed air jet located about 80 mm from the sample is directed to the surface of the deposit after the projection, to control cooling. The spray parameters used are given in Table III.

C. Microstructural Characterization

The surface of samples was ground using SiC paper with grit sizes and finally polished with alumina. Microstructures of the initial wire and produced coatings were observed on its surface using a scanning electron microscope (SEM) from Japanese (JEOL JSM-6360LV) in high vacuum. Chemical composition of coatings was analyzed using an energy dispersive spectroscopy (EDS).

D. XRD Diffraction

The X-ray diffraction patterns were recorded using diffractometer type X'PERT PRO MRD of PANalytical, equipped with a copper anode X-ray tube. The components $K\alpha2$ are not filtered by a monochromator graphite curve mounted in the secondary beam. The strong presence of defects in these materials creates a significant background noise; to improve counting statistics and increase the ratio pics/continuous background, an acquisition time of 40 seconds per angular step of 0.04 deg and a count time of 5 seconds per step has been used in the interval ranging between 10 deg and 90 deg(2θ). The identification of the crystal phases present was made by comparison of the observed lines with those appropriate phases contained in the database PDF2

E. Microhardness Test

Vickers microhardness measurement was performed on the as-polished surface of coatings using a microhardness tester type Zeiss under a load of 200 g and a dwell time of 30 seconds. An average hardness was calculated from 10 indents per specimen.

F. Friction and Wear Test

Friction test was performed with a pin-on-disk arrangement. The schematic of the tribometer is shown in (Figure 2(a)). This test was effectuated under different loads (5, 10, 15, 20, and 30 N) with a sliding distance of 1000 m of the duration 30 minutes, sliding speed of 0.5 m/s, and a wear track diameter of 3 cm (Figure 2(b)).

Table I.   Chemical Composition of Substrate E335

C	Mo	Cu	Ni	Mn	Fe	P	Si	V	S
0.1	0.007	0.119	<0.03	0.231	Bal	0.050	0.044	<0.01	0.010

Table II. Chemical Compositions of Materials Used

Materials	Al_2O_3	TiO_2	ZrO_2	Others
Al_2O_3-TiO_2 (AT-13)	87	12.7	—	0.3
(AZ-25) Disk 1	75	—	24.5	0.5
(AT-3) Disk 2	97	2.8	—	0.2
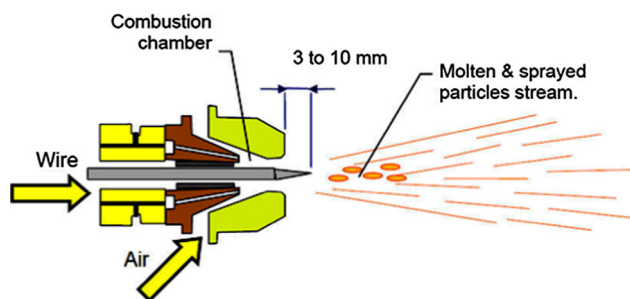
Fig. 1—Schema of operating of a flame-gun wire.

Table III. Spray Parameters

Projection Parameters	Al_2O_3-TiO_2
Gas	acetylene
Wire's speed (mm/s)	10
Rate of flow wire (kg/h)	1.25
Pressure air (MPa)	4.5×10^3
Pressure gas (MPa)	4×10^3
Pressure oxygen (MPa)	1.2×10^3
Height Bille oxygen (mm)	70
Height Bille gas (mm)	60
Spray distance (mm)	120 to 150
Spray angle	90 deg

The coated steel substrate, formed the pins in the system, was machined into cylinders of 10 mm diameter and 20 mm length. A ceramic disk of 30 cm diameter was employed as the counter body with a new disk being used for each test. Both pin and disk samples were cleaned with ethanol and dry compressed air before and after testing. In order to study the wear behavior of coatings in severe conditions, the tests were carried out without any lubrication. The wears experienced by the samples during the tests were determined by weighting each sample before and after the test. The weight loss suffered by the pins was measured using electronic weighing balance having an accuracy ±0.01 mg. In addition, the friction coefficient is estimated directly by an acquisition system (3D piezoelectric sensor).

The wear rate is calculated using the following equation:

$$k_v = \frac{\Delta m}{N_c}.$$ [1]

K_v wear rate, Δm weight loss, N_c number of cycles.

The value of the static friction coefficient is obtained by the equation below:

$$\mu = \frac{F_t}{N}.$$ [2]

F_t tangential force, N normal force.

Tribological tests were performed according two contact couples:

– Couple 1: Pin coated with Al_2O_3-TiO_2 (AT-13)/ ceramic disk Al_2O_3-ZrO_2 (AZ-25).
– Couple 2: Pin coated with Al_2O_3-TiO_2 (AT-13)/ ceramic disk Al_2O_3-TiO_2 (AT-3).

The condition tests are as follows:
Relatively dry environment: 293 K to 296 K (20 °C to 23 °C).
Normal loads: 5 to 30 N.
Sliding speed: 0.5 m/s.
Sliding duration: 30 minutes.
Sliding distance: 1000 m.
The roughness measurements were made with a 3D profilometer type Altisurf 500. It is an optical metrology equipment which is used to study the surface topography. It is a powerful tool in the establishment of relationship between surface states, coating, micro-dimension. Six measurements are taken per sample by step distance of 4.8 mm. In fact, coatings are in different roughnesses due to their mode of construction.

III. RESULTS AND DISCUSSION

A. Microstructural Characterization

Figure 3 shows the morphology of the wire in AT-13. It has a microstructure of micrometric particles, of different sizes, with the fracture planes and pores on their surface, typical of materials subjected to a melting process, and subsequently to a reduction size by grinding.

The SEM observations of the coating alloy Al_2O_3-13pctTiO_2 (AT-13) obtained by oxyacetylene flame spray showed a dense microstructure, compact and complex of several phases with the presence of porosities and unmelted particles (Figure 4). This microstructure is constituted by lamellae and globular pores and has not cracks because the stresses produced during the formation of these multilayers are not sufficient to produce it.[22] Also, the coating has a low porosity which can be associated with the effect of the higher speed in flight of the melted particles from the wire and it is due to the high pressure of air jet uses, from this higher impact speed it results a better spreading lamellae.

According to Figure 5, which is a back-scattered SEM photograph of the Al_2O_3-TiO_2 (AT-13) coatings, EDS analysis has identified the light gray area as a matrix of Al_2O_3 lamella (Figure 6(a)); the other phase is dark gray area that contains aluminum, oxygen, and traces of titanium of chemical formula $(Al_2O_3)_{5.333}$
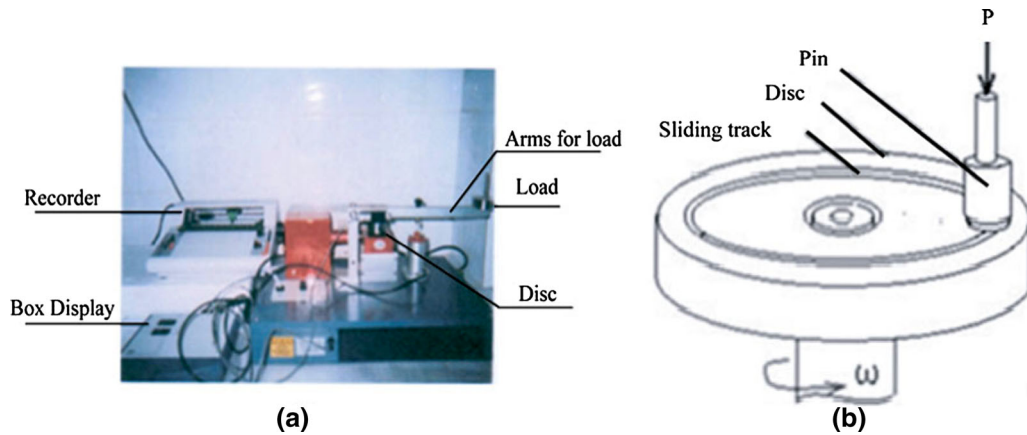
Fig. 2—(*a*) Schematic representation tribometer TE 91, (*b*) contact pin-on-disk configuration.
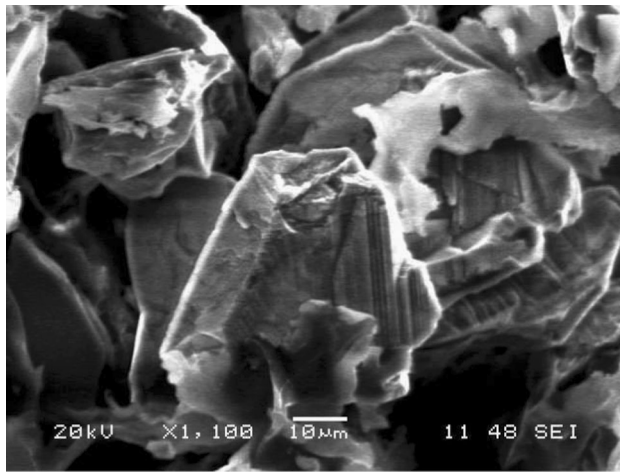

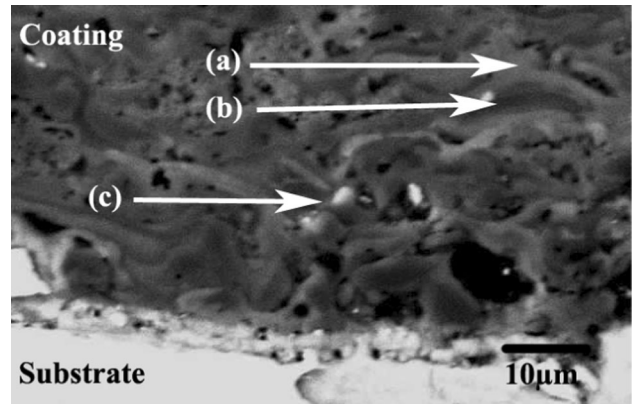Fig. 3—SEM (secondary electron) image of Al_2O_3-13 wt pct TiO_2.

Fig. 5—SEM (backscattered electron) image of the Al_2O_3-TiO_2 (AT-13) coating showing three different phases: (*a*) light gray, (*b*) dark gray, and (*c*) white area.
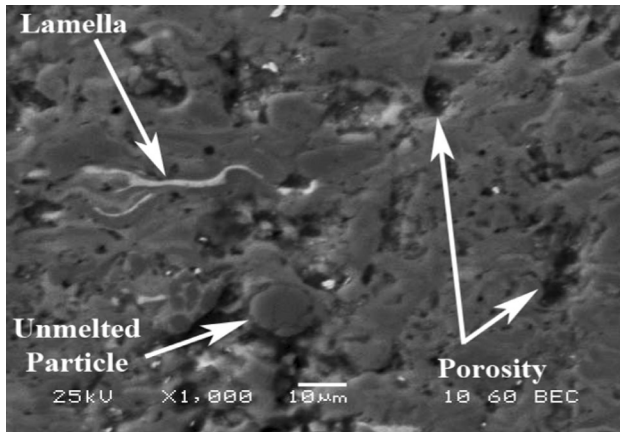

Fig. 4—SEM (back scattering electron) image of the cross section of Al_2O_3-TiO_2 (AT-13) coating.

B. *X-ray Diffraction Analysis (XRD)*

Figure 6 shows the diffraction patterns of X-ray of the wire alloy Al_2O_3-TiO_2 (AT-13) and coating obtained by spraying flame wire.

Figure 7(a) shows the diffractogram obtained exclusively from the wire Al_2O_3-TiO_2 (AT-13). The observed peaks are revealed the presence of three phases: a majority phase of α-Al_2O_3 rhombohedral structure (JCPDS No 046-1212), secondary phase is Al_2TiO_5 orthorhombic structure (JCPDS No 01-081-0030) with small amount of rutile TiO_2 tetragonal structure (JCPDS No 01-077-0440). The refinement crystalline parameters of the three phases present in the wire Al_2O_3-TiO_2 (AT-13), taking into account the shift of the spectrum related to the sample position, give the following values shown in Table IV.

The XRD spectrum of Al_2O_3-TiO_2 (AT-13) coatings (Figure 7(b)) revealed also the presence of phases of α-Al_2O_3 and Al_2TiO_5, but one notes the disappearance of TiO_2 phase which is substituted by the formation of a new metastable phase γ-Al_2O_3 cubic structure (JCPDS No 01-074-2206). The crystalline parameter of this new cubic phase is 7.9060 Å. Indeed, the time of elaboration
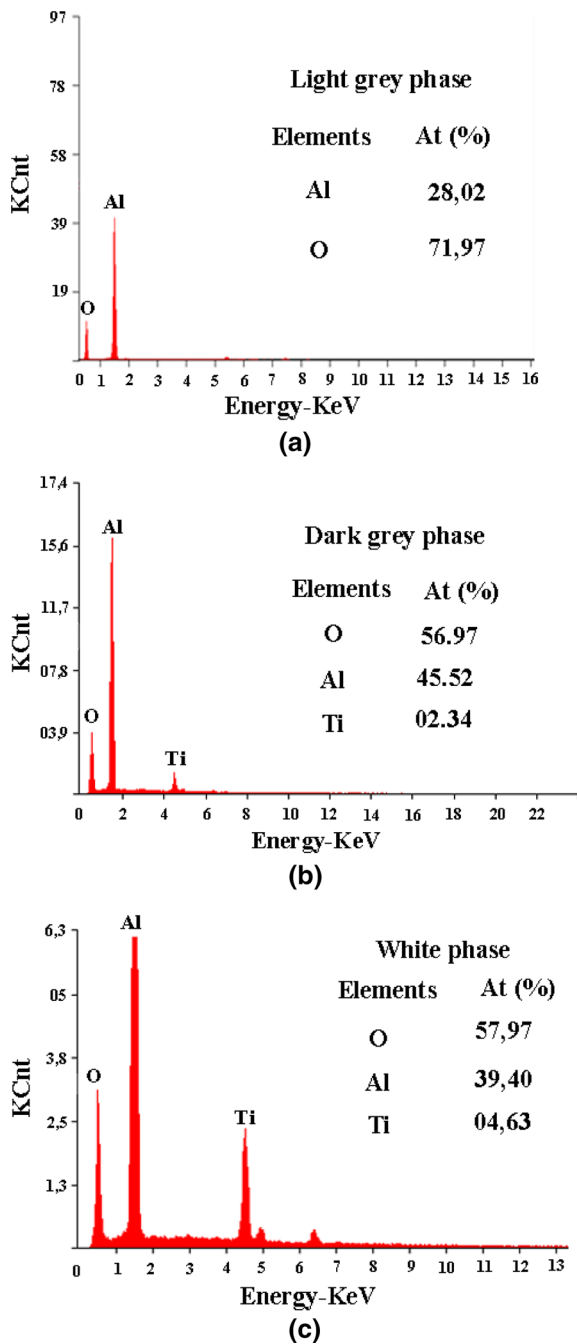
corresponding to the metastable phase γ-Al_2O_3 (Figure 6(b)) and the white area phase (Figure 6(c)) shows also the presence of aluminum, oxygen, and titanium with atomic ratio corresponding to the Al_2O_5Ti.

(a)

(b)

(c)

Fig. 6—EDS analysis of coating Al_2O_3-TiO_2 (AT-13): (*a*) light gray phase, (*b*) dark gray phase, (*c*) white phase.

the coating from the wire Al_2O_3-TiO_2 is not enough to form oxides of titanium or others phases that contain Ti atoms and consequently, the Ti atoms are dissolved on phase γ-Al_2O_3.[23–25]

C. Microhardness

The microhardnesses of the various materials used substrate E335, coating alloy Al_2O_3-TiO_2 (AT-13) and opposing disks which form the contact couples (Al_2O_3-TiO_2 (AT-3) and Al_2O_3-ZrO_2 (AZ-25)) were measured by Vickers indentation with a load of 200 g during

30 seconds. For each processing, the calculated average standard deviation is based on the average of 20 measurements. The results of Vickers pyramid hardness are illustrated by the histogram in Figure 8.

These tests revealed that the microhardness of the coating Al_2O_3-TiO_2 (AT-13) is three times higher than antagonist disk 1 of Al_2O_3-ZrO_2 (AZ-25): 1280 ± 66 HV0.2 (AT-13) against about 563 ± 25 HV0.2 (AZ-25). This gap can be due to the influence of the quantity of porosity and differences between hardness of reinforcement elements of titanium in Al_2O_3-TiO_2 and zirconium for Al_2O_3-ZrO_2. However, the microhardness values of coating Al_2O_3-TiO_2 (AT-13) are nearly equal to other antagonist disk 2 of alloy Al_2O_3-TiO_2 (AT-3): 1280 ± 66 HV0.2 (AT-13) against about 1326 ± 64 HV0.2 (AT-3). In principle, the microhardness of Al_2O_3-TiO_2 coatings depends essentially on their composition, decreasing linearly with the TiO_2 content.[19] The phases in the coatings Al_2O_3-TiO_2 (AT-13) are mainly constituted of both alpha-alumina (α-Al_2O_3) and gamma-alumina (γ-Al_2O_3) while (Al_2TiO_5) phase has lower hardness and mechanical resistance than alpha- and gamma-alumina.[20,22,26]

D. Friction Coefficient and Wear Rate

Figure 9 shows the effect of load on variation of friction coefficient for two contacts studied. The tribological results showed that the two curves corresponding to the variation of the friction coefficient in function as the load of the two contacts are nearly identical. This is mainly due to the asperities which generates a tangential resistant force being next to the normal force. The first part of the curves (5 to 10 N) corresponds to the accommodation phase of surfaces between disk and pin when the contact is established. After that, the friction coefficient decreases progressively until being stabilized around a value of 0.7 under 30 N load. Generally, for all test conditions done, the friction coefficient studied of the couples have the same shape but the values varied. This can be explained by the different changes microstructures during the test. However, it is interesting to focus this study on the variation of the friction coefficient of the two couples in function as sliding time for loads of 5 and 30 N (Figure 10).

The first part of all curves (Figure 10) corresponds to accommodation phase which is observed during the first five minutes under applied loads (5 and 30 N). The only way that the material could be removed from the sample surface is cracking and spread by the cyclical contact fatigue; however, it appears that contact is not high enough to induce these stress. This transition phase can be explained by the increasing of the tangential force generated then the stresses which cannot cut the asperities between the first bodies by shearing mechanism at the contact surfaces. After this phase, the results obtained from (Figure 10(a)) gave an average friction coefficient of about 0.92 for the two couples when they slide under 5 N. Similarly, the results obtained from (Figure 10(b)), under high load 30 N, gave a friction coefficient of about 0.65 for couple 2 and only 0.46 was recorded for couple 1. These values were determined by
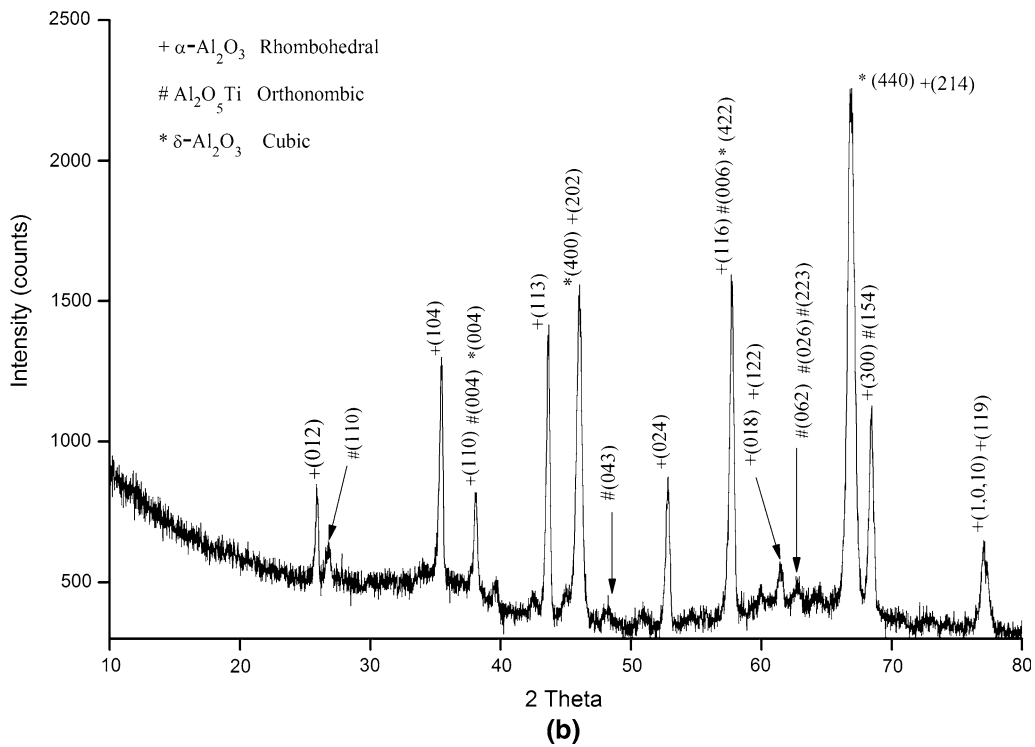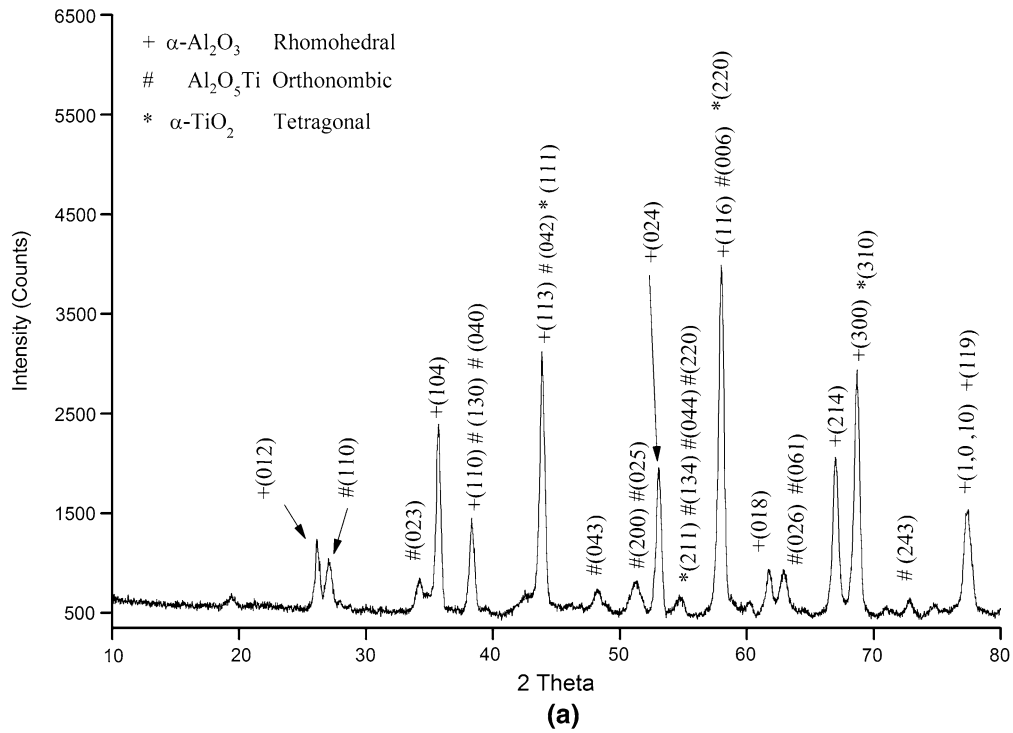
Fig. 7—XRD diffraction patterns of Al₂O₃-TiO₂ (AT-13). (*a*) Wire, (*b*) coating.

Table IV.   Parameters Crystalline of the Phases Forming the Wire Al₂O₃-TiO₂ (AT-13)

Parameters Crystalline (Å)	Al₂O₃rhombohedral	Al₂TiO₅orthorhombic	TiO₂tetragonal
a	4.7587	3.5910	4.5934
b	4.7587	9.4290	4.5934
c	12.9929	9.6360	2.9575
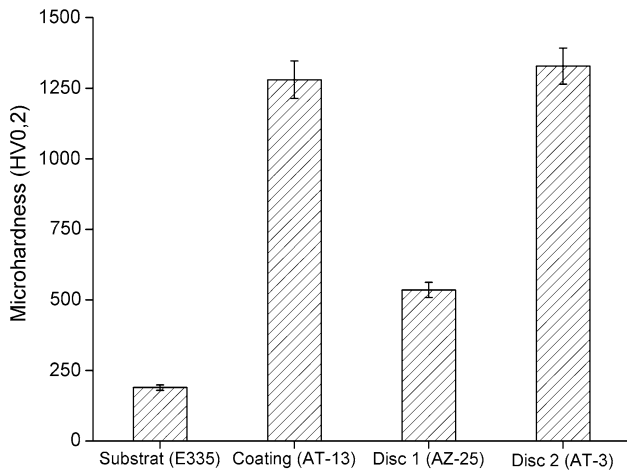
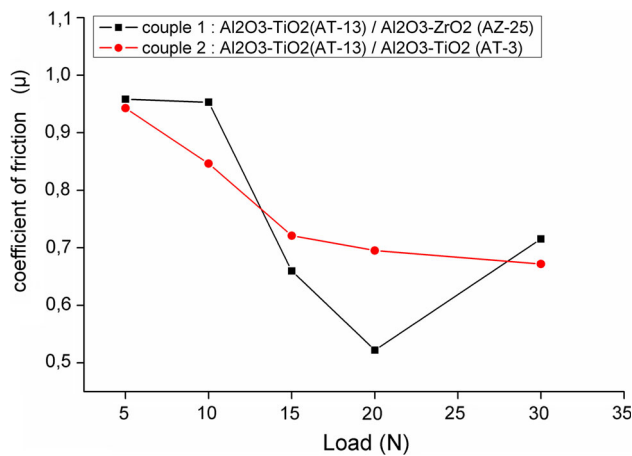Fig. 8—Microhardness of different materials used. Longitudinal bars show maximum and minimum microhardness.

Fig. 9—Evolution of friction coefficient as a function load.

(a)

(b)

Fig. 10—Evolution of the coefficient of friction of the coatings as function sliding time. (a) Under 5 N load, (b) under 30 N load.

averaging the friction coefficients over the stabilization stage of each test. From this, we can say clearly that the pressure affects the variation of friction coefficient as function sliding time. The direct contact between the surfaces of the two couples studied in the stabilization zone is characterized by a sliding friction which cannot generate shearing of the asperities. This is due to not enough stress able to form a shearing mode. Therefore, the friction coefficient is constant between the opposing surfaces (pin and disk). While for the couple 1 (Figure 10), a turbulence is noted at about the seventh minute which can probably explain by the debris rejected during the contact thus forming a third body which affects the behavior of the friction.

Figure 11 illustrates the variation of the wear rate as a function of load at a sliding speed of 0.5 m/s and a sliding duration of 30 minutes for the two couples.

In this figure, it can be seen that the wear rates are almost increasing with the increase in load and those of coatings of couple 2 increase more slowly. This can be
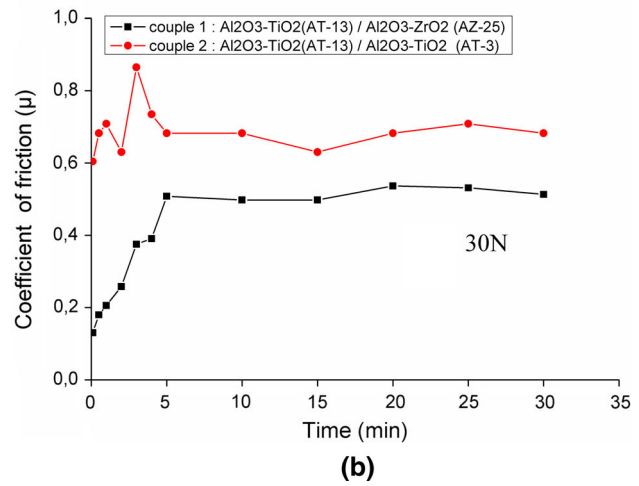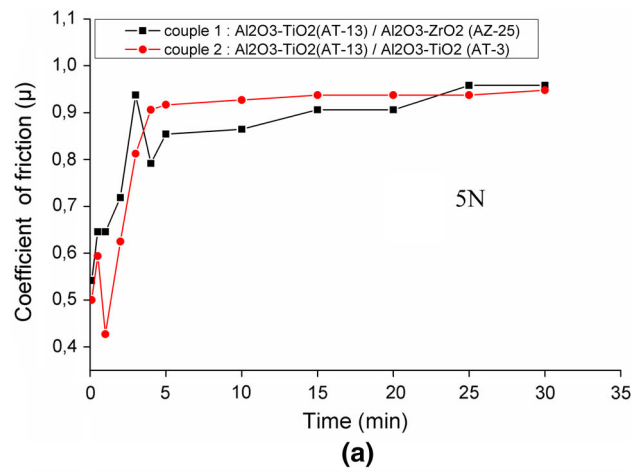
explained by wear divided between coating (AT-13) and disk 2 (AT-3) for the couple 2. Therefore, the chemical compositions of the two surfaces (pin and disk 2) are very nearly. Contrary of couple 1, the two antagonist materials (pin and disk 1) have different characteristics (See Section II–A). Generally, the wear tests induce large deformations and cause the appearance of the particles of third body (Figure 12). Some of these particles are rapidly rejected from the friction track and others are oxided according to the contact temperature, which increases with the increase of the load. These particles were presented at different forms that affect the wear properties of the coating by changing its state of stress. Through these tribological tests, we can conclude that the couple two with nearly chemical compositions spray-coated (AT-13) and disk 2 exhibited much higher wear resistance that the couple 1 although they have sliding coefficients of friction nearly. We can also conclude that the load affects the tribological proprieties of the coating by changing its stress state on the worn surfaces.

E. Roughness Profile

Figure 13 shows profile of the roughness of the pin before the tribological test. It is clear that for polished surfaces, the asperities are scarce and their average roughness Ra is in the order of 6.5 μ.

In the following, we present the variation of the roughness of the pin coated with Al_2O_3-TiO_2 (AT-13) as the function of the load (Figure 14).
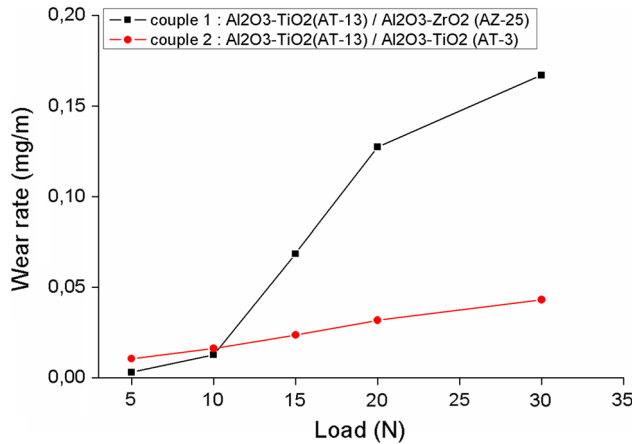
In this figure, the roughness coatings values of two couples studied show a significant gap at the beginning of the test that is about 5 μm. This difference decreases with the increase of the load to 20 N and the roughness of the two couple tends to stabilize during the test. It can be explained by the appearance of a relief which thus generates a roughness profile. Through these results, we can say that the load applied on coatings affects the roughness profile on the surfaces. After the tribological tests, we found that the
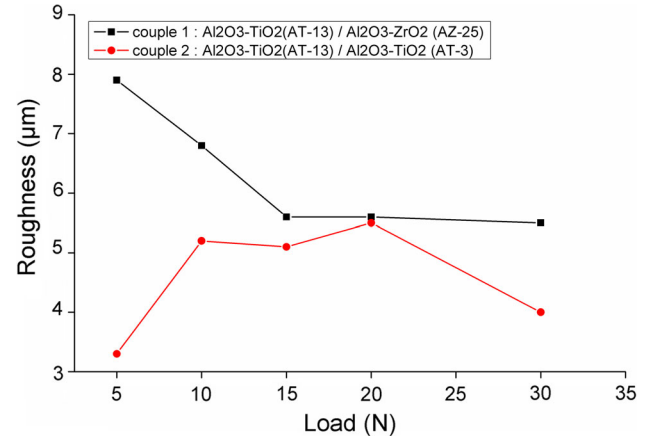

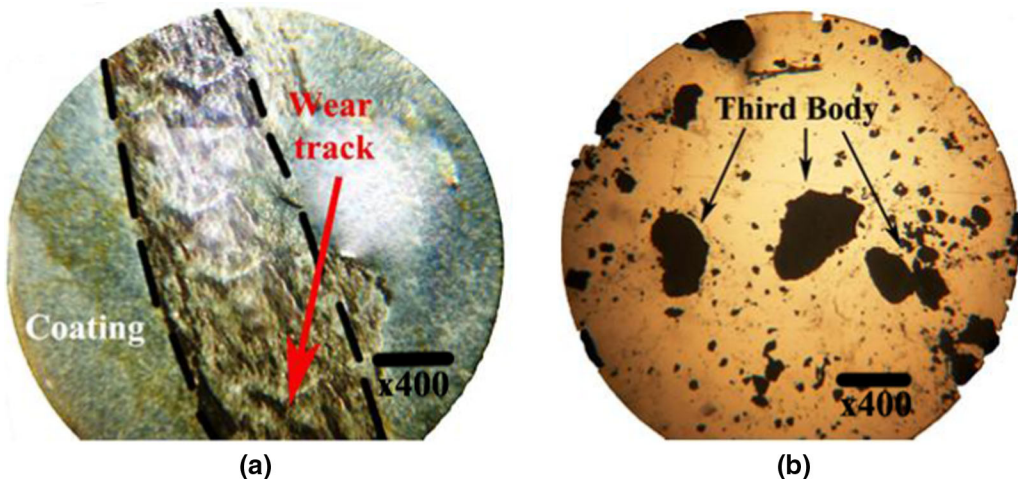Fig. 11—Evolution of the wear rate of the coatings as function load.

Fig. 14—Evolution of the roughness of the coatings as function load.

Fig. 12—Optical microscope image of coating Al_2O_3-TiO_2 (AT-13): (a) wear track, (b) third body.
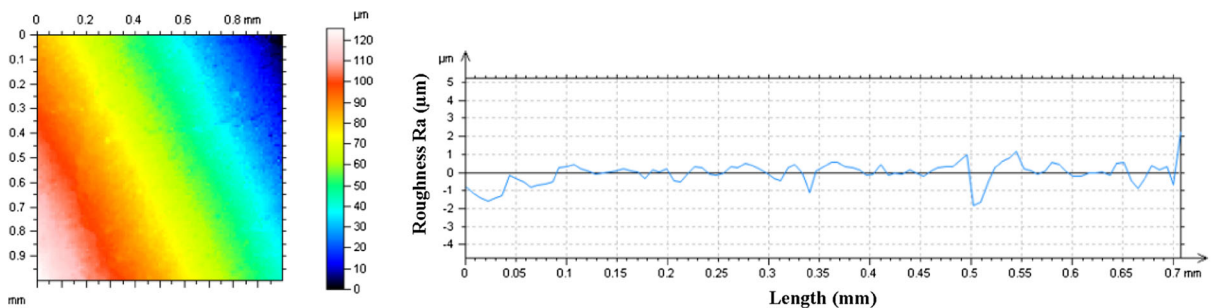

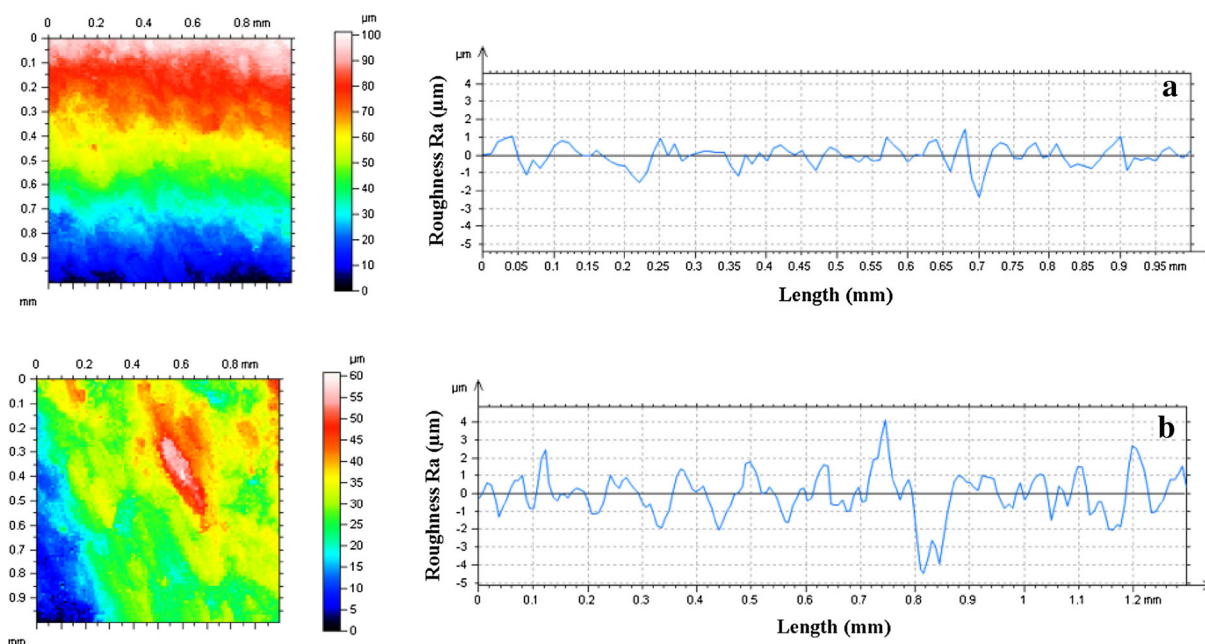Fig. 13—Roughness profile before tribological test.

Fig. 15—Roughness profile after tribological test. (*a*) Couple 1, (*b*) couple 2.

roughness profile for coatings of two couples under the load of 30 N (Figure 15) varies on average 3.5 to 5.5 μm for couple 2 and couple 1, respectively.

The observations of the wear tracks of pins show that the depth of the asperities does not exceed the initial roughness of the coatings. It can therefore affect the tribological properties.[27] However, the surface roughness is the same for both coatings before testing. After the test, the coatings of the couple 1 have higher profile roughness than those coatings of the couple 2 (5.5 μm couple 1 against 3.5 μm to the couple 2). In the case of Couple 1, the cut mode occurs by shearing thus generating debris which was constituted of hard and abrasive particles which cause increasing wear (Figure 15). Contrary to couple 2, the contact mode is characterized by a sliding friction which generates a smaller surface roughness, so the pins of this couple are less worn.

IV. CONCLUSIONS

This aim study is to produce coatings ceramic Al_2O_3-TiO_2 (AT-13) using the thermal spray flame technique in order to improve the wear resistance. On the basis of the obtained results in the present investigation, the following conclusions can be drawn:

1. The SEM microstructures showed that the coatings Al_2O_3-TiO_2 (AT-13) have a homogeneous lamellar morphology and low content of porosities.
2. The XRD spectrum of the wire showed a majority phase of α-Al_2O_3 rhombohedral structure and secondary phase of Al_2TiO_5 orthorhombic structure with little traces of TiO_2 (rutile) tetragonal structure and the spectrum of the coating revealed the disappearance of TiO_2 replaced by the formation of a new metastable phase γ-Al_2O_3 cubic structure.

3. Microhardness tests revealed that the Al_2O_3-TiO_2 coating (AT-13) is almost three times harder than the disk 1 Al_2O_3-ZrO_2 (AZ-25) and has a nearly hardness that the disk 2 Al_2O_3-TiO_2 (AT- 3).
4. The tribological results showed that the contact pressure applied affects the variation of the friction coefficient in function of time and that it decreases with the increase of the normal force of contact. We can also conclude that the couple two with nearly chemical compositions spray-coated (AT-13) and disk 2 exhibited much higher wear resistance that the couple 1 although they have sliding coefficients of friction nearly.
5. The observations of the wear tracks of pins showed that the depth of the asperities does not exceed the initial roughness of the coatings. In the case of Couple 1, the cut mode occurs by shearing thus generating debris which are constituted of hard and abrasive particles which cause increasing wear. Contrary to couple 2, the contact mode is characterized by a sliding friction which generates a smaller surface roughness, so the pins of this couple are less worn.

REFERENCES

1. S. Brossard, P.R. Munroe, A.T.T. Tran, and M.M. Hyland: *Surf. Coat. Technol.*, 2010, vol. 204 (16–17), pp. 2647–56.
2. L. Wang, Y. Wang, X.G. Sun, J.Q. He, Z.Y. Pan, Y. Zhou, and P.L. Wu: *Mater. Des.*, 2011, vol. 32 (1), pp. 36–47.
3. K. Alamara, S.S. Samandari, P.R. Stoddart, and C.C. Berndt: *Surf. Coat. Technol.*, 2011, vol. 206 (6), pp. 1180–87.
4. M. Wang and L.S. Leon: *Surf. Coat. Technol.*, 2007, vol. 202 (1), pp. 34–44.
5. A. Keyvani: *J. Alloys. Compd.*, 2015, vol. 623, pp. 229–37.
6. M. Vicent, E. Bannier, P. Carpio, E. Rayón, R. Benavente, M.D. Salvador, and E. Sánchez: *Surf. Coat. Technol.*, 2015, vol. 268, pp. 209–15.
7. A. Rico, J. Rodriguez, E. Otero, P. Zeng, and W.M. Rainforth: *Wear*, 2009, vol. 267 (5–8), pp. 1191–97.

8. Y. Yang, Y. Wang, W. Tian, D.R. Yan, J.-X. Zhang, and L. Wang: *Mater. Des.*, 2015, vol. 65, pp. 814–22.
9. R.S. Lima, B.R. Marple, K.A. Khor, H. Li, and P. Cheang: *Mater. Sci. Eng. A*, 2005, vol. 396 (1–2), pp. 181–187.
10. V.P. Singh, A. Sil, and R. Jayaganthan: *Mater. Des.*, 2011, vol. 32 (2), pp. 584–591.
11. V. Bolleddu, V. Racherla, and P.P. Bandyopadhyay: *Mater. Des.*, 2014, vol. 59, pp. 252–63.
12. B. Torres, M.A. Garrido, A. Rico, P. Rodrigo, M. Campo, and J. Rams: *Wear*, 2010, vol. 268 (5–6), pp. 828–36.
13. M.H. Enayati, F. Karimzadeh, M. Jafari, A. Markazi, and A. Tahvilian: *Mater. Sci. Eng. A*, 2013, vol. 578, pp. 46–53.
14. S. Devaraj, S. Sankaran, and R. Kumar: *Acta Metall. Sin.*, 2013, vol. 26, pp. 761–71.
15. R.J.K. Wood: *Int. J. Refract. Met. Hard. Mater.*, 2010, vol. 28 (1), pp. 82–94.
16. M.A. Farrokhzad and T.I. Khan: *Oxid. Metal*, 2014, vol. 81 (1–2), pp. 267–85.
17. M. Priest: *Tribol. Ser.*, 2003, vol. 41, pp. 739–48.
18. S. Nourouzi: Ph.D. Thesis, University of Limoges, French, 2004.
19. V. Fervel, B. Normand, and C. Coddet: *Wear*, 1999, vol. 230 (1), pp. 70–7.
20. K.A. Habib, J.J. Saura, C. Ferre, M.S. Damra, E. Gimenez, and L. Cabedo: *Surf. Coat. Technol.*, 2006, vol. 201 (3-4), pp. 1436–43.
21. J. Ahn, B.H. Wang, E.P. Song, S. Lee, and N.J. Kim: *Metall. Mater. Trans. A*, 2006, vol. 37A, pp. 1851–61.
22. F. Vargas, H. Ageorges, P. Fournier, P. Fauchais, and M.E. López: *Surf. Coat. Technol.*, 2010, vol. 205 (4), pp. 1132–36.
23. A. Gaard, P. Krakhmalev, J. Bergström, J.H. Grytzelius, and H.M. Zhang: *Wear*, 2009, vol. 267 (1–4), pp. 387–93.
24. M. Wang and L. Shaw: *Surf. Coat. Technol.*, 2007, vol. 202 (1), pp. 34–44.
25. D. Goberman, Y.H. Sohn, L. Shaw, E. Jordan, and M. Gell: *Acta Mater.*, 2002, vol. 50 (5), pp. 1141–52.
26. R. Yilmaz, A.O. Kurt, A. Demir, and Z. Tatli: *J. Eur. Ceram. Soc.*, 2007, vol. 27 (2–3), pp. 1319–23.
27. C.-W. Kim, J.-H. Choi, H.-J. Kim, D.-W. Lee, C.-Y. Hyun, and S.-M. Nam: *Ceram. Inter.*, 2012, vol. 38 (7), pp. 5621–27.